

Electronic structure of the Kagomé lattice compound $\text{Rb}_2\text{Ni}_3\text{S}_4$

S. Nawai, K. Okazaki, T. Mizokawa, and A. Fujimori

Department of Complexity Science and Engineering and Department of Physics, University of Tokyo, Bunkyo-ku, Tokyo 113-0033, Japan

K. Hondou, Y. Fujiwara, and K. Iio

Department of Physics, Graduate School of Science and Engineering, Tokyo Institute of Technology, Meguro-ku, Tokyo 152-8551, Japan

M. Usuda* and N. Hamada

Department of Physics, Faculty of Science and Technology, Science University of Tokyo, Noda-shi, Chiba 278-8510, Japan

(Received 18 August 2003; published 7 January 2004)

We have studied the electronic structure of the layered Kagomé lattice compound $\text{Rb}_2\text{Ni}_3\text{S}_4$ by photoemission spectroscopy and comparison of the results with band-structure and configuration-interaction cluster-model calculations. The band-structure calculation reproduced the gross features of the experimental spectra but could not reproduce the weak satellite feature, and predicted the narrow peak of Ni $3d$ character just below the Fermi level (E_F) to be too strong. On the other hand, the cluster-model calculation assuming the low-spin ($S=0$) ground state reproduced the satellite but failed to predict the same peak just below E_F at the correct energy position. Angle-resolved photoemission measurements revealed momentum dispersions for the S $3p$ -derived and Ni $3d$ -S $3p$ hybridized bands, in agreement with the band-structure calculation, whereas the Ni $3d$ -derived band just below E_F was found to be dispersionless, unlike the result of the band-structure calculation. We conclude that $\text{Rb}_2\text{Ni}_3\text{S}_4$ is a moderately correlated, strongly p - d hybridized system.

DOI: 10.1103/PhysRevB.69.045103

PACS number(s): 79.60.Bm, 75.20.Ck, 71.28.+d, 71.20.Nr

I. INTRODUCTION

The series of Ni sulfides exhibit interesting physical properties arising from electron correlation between the Ni $3d$ electrons and hybridization between the Ni $3d$ and S $3p$ orbitals.¹ Hexagonal NiS undergoes a first-order insulator-to-metal transition under high pressure, with increasing temperature, or by Se substitution for S.² Pyrite-type NiS₂ exhibits pressure-, temperature-, and Se-substitution-induced insulator-to-metal transitions but with a more complicated phase diagram including an antiferromagnetic metallic phase.³ The pseudoternary compound $\text{BaCo}_{1-x}\text{Ni}_x\text{S}_2$ with a layered structure exhibits a metal-insulator transition as a function of composition or temperature.⁴

Layered transition-metal sulfides have attracted considerable interest because of their applications as cathode materials in Li-ion cells.^{6,7} The layered Ni sulfide $\text{Rb}_2\text{Ni}_3\text{S}_4$ studied here is particularly interesting because the Ni²⁺ ions form a Kagomé lattice as indicated in Fig. 1.⁵ Each Ni ion is located at the center of four S atoms in a square planar configuration, and the NiS₄ units are linked to form six-membered rings. On the Kagomé lattice, the Ni spins, if they are coupled antiferromagnetically, form a geometrically frustrated spin system. Indeed, there have been controversial reports on the magnetic properties of $\text{Rb}_2\text{Ni}_3\text{S}_4$.^{8,9} Weak ferromagnetism was reported at low temperatures, and was attributed to the frustration of $S=1$ spins¹⁰ or to magnetic impurities dissolved in the nonmagnetic band insulator.¹¹ In subsequent work,¹² the same material was shown to be diamagnetic if water was not used to remove the flux used in the crystal growth, while it became weakly ferromagnetic if water was used. It remains unclear why the latter sample exhibits weak ferromagnetism. The role of water intercalation in layered compounds has attracted recent interest due to the discovery

of superconductivity in $\text{Na}_x\text{CoO}_2 \cdot n(\text{H}_2\text{O})$.¹³ The unusual weak ferromagnetism in water-treated $\text{Rb}_2\text{Ni}_3\text{S}_4$ may therefore be worthwhile for further studies.

The electrical resistivity of $\text{Rb}_2\text{Ni}_3\text{S}_4$ shows three characteristic temperature ranges:¹² above 100 K the activation energy is 0.4 eV while between 30 K and 100 K it is 0.05 eV; the resistivity becomes temperature independent below 30 K. The resistivity shows strong anisotropy due to the layered crystal structure, namely, the out-of-plane resistivity is about two orders of magnitude higher than the in-plane resistivity.¹² If intercalation and/or de-intercalation of alkali-metal ions in $\text{Rb}_2\text{Ni}_3\text{S}_4$ were realized, electron and/or hole doping would become possible in the Kagomé lattice and interesting physical properties would be expected.

In the present work, we studied $\text{Rb}_2\text{Ni}_3\text{S}_4$ by photoemission spectroscopy combined with band-structure and cluster-model calculations, in order to reveal its electronic structure which forms the basis for its magnetic and electrical properties. We shall focus on the Ni $3d$ -S $3p$ hybridization, the Coulomb interaction among the Ni $3d$ electrons, and the energy band dispersions, in order to see how the Coulomb

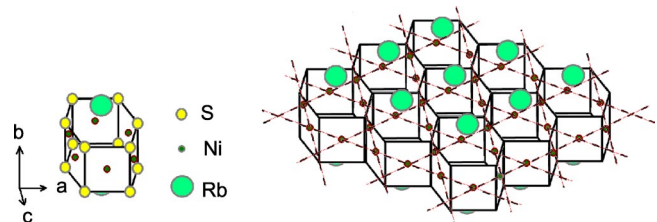


FIG. 1. (Color online) Crystal structure of $\text{Rb}_2\text{Ni}_3\text{S}_4$. The two-dimensional hexagonal arrays shown in the right panel are stacked to form the three-dimensional crystal.

interaction and the $p-d$ hybridization affect the electronic properties of $\text{Rb}_2\text{Ni}_3\text{S}_4$.

II. EXPERIMENT

Single crystals of $\text{Rb}_2\text{Ni}_3\text{S}_4$ were prepared by the flux method starting from Rb_2CO_3 (99%), Ni (99%), and S (99%), mixed in the ratio 5:1:12. In order to remove the flux, the surface of the crystal was mechanically peeled off without using water. Details of the sample preparation are given in Ref. 12. X-ray photoemission spectroscopy (XPS) and ultraviolet photoemission spectroscopy (UPS) measurements were performed using a spectrometer equipped with a Mg x-ray source (Mg $K\alpha$: $h\nu=1253.6$ eV), a He discharge lamp (He I: $h\nu=21.2$ eV, He II: $h\nu=40.8$ eV), and a VSW CLASS-150 hemispherical analyzer. Inverse-photoemission spectroscopy or Bremsstrahlung isochromat spectroscopy (BIS) measurements were done using a crystal monochromator tuned for photons of $h\nu=1486.6$ eV. The base pressure of the spectrometer was $\sim 10^{-10}$ Torr. All the measurements were made at room temperature. The resolution of XPS, BIS, and UPS was ~ 0.7 eV, ~ 0.8 eV, and 50–100 meV, respectively. In order to obtain clean surfaces, the samples were cleaved *in situ* in the ultrahigh vacuum of the spectrometer using the “top-post” method. The acceptance angle of the electron analyzer was about $\sim \pm 8^\circ$ for angle-integrated photoemission spectroscopy (AIPES) and $\sim \pm 1^\circ$ for angle-resolved photoemission spectroscopy (ARPES). Crystal orientation was determined by Laue diffraction. Most of the measurements were done in the AIPES mode unless otherwise stated.

III. RESULTS AND DISCUSSION

The valence-band photoemission spectra of $\text{Rb}_2\text{Ni}_3\text{S}_4$ obtained using different photon energies, namely, XPS, He II UPS, and He I UPS, are shown in Fig. 2. Various features in the spectra are marked as A, B, C, D, E, and F. Since the relative photoionization cross sections of the Ni $3d$ and S $3p$ atomic orbitals change with photon energy, the changes in the relative intensities of those spectral features reflect their different atomic orbital characters. With increasing photon energy from He I to He II, the intensities of features C, D, and E dramatically decrease. Because the Cooper minimum in the S $3p$ photoionization cross section occurs at ~ 50 eV, the present observation indicates the dominance of S $3p$ character in features C, D, and E. Therefore, one can conclude that C, D, and E are derived from the S $3p$ atomic orbitals, while A and B are primarily derived from the Ni $3d$ atomic orbitals.

For more detailed analysis, the density of states (DOS) of $\text{Rb}_2\text{Ni}_3\text{S}_4$ obtained from first-principles band-structure calculation is employed. The calculation was carried out using the full-potential linear-augmented-plane-wave (FLAPW) method based on the local-density approximation (LDA). Because there has been no report on the exact positions of the Rb and S atoms in $\text{Rb}_2\text{Ni}_3\text{S}_4$, their approximate positions were estimated from the crystal structure data of $\text{Cs}_2\text{Ni}_3\text{Se}_4$, which has the same space group as $\text{Rb}_2\text{Ni}_3\text{S}_4$.⁵ In the

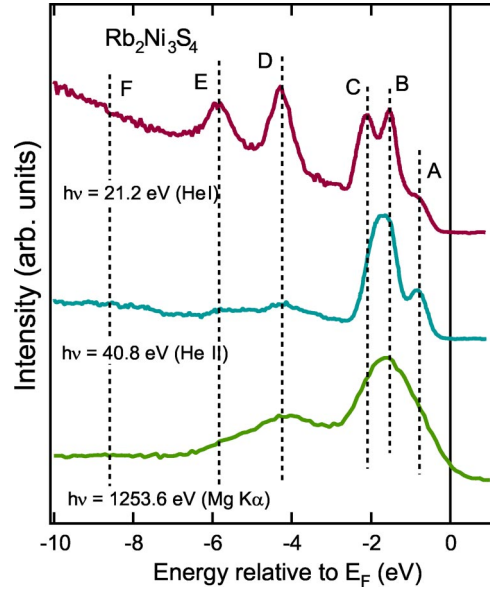


FIG. 2. (Color online) Valence-band photoemission spectra for various photon energies.

valence-band region (from 2 eV to -10 eV), the total DOS is dominated by Ni $3d$ and S $3p$ states. Calculation showed that the centers of the Ni $3d$ and S $3p$ bands are separated only by ~ 3 eV and these bands are strongly hybridized with each other.¹² In the following analysis, therefore, we shall consider only two contributions, namely, the Ni d and S p partial DOS's. In order to take into account the different photoionization cross sections of the Ni $3d$ and S $3p$ atomic orbitals, we calculated a weighted average of the Ni d and S p partial DOS's in the valence-band spectra using atomic orbital photoionization cross sections.¹⁴ The straightforward use of the atomic orbital cross sections is usually insufficient for this purpose, however, because the partial DOS depends on the radius of the atomic sphere used for charge integration and also because solid-state effects may change the cross sections. Usually, the anion p partial DOS is severely underestimated because of the small muffin-tin radius in spite of the large ionic radius. Therefore, we assumed that the contribution of S $3p$ is ~ 5 times larger than the atomic orbital photoionization cross section multiplied by the calculated partial DOS.¹⁵ The calculated spectra were broadened to simulate the photohole lifetime broadening with an energy dependent Lorentzian full width at half maximum (FWHM) $\Gamma=0.1(E-E_F)$ eV for UPS and $\text{FWHM} \approx 0.2+0.15(E-E_B)$ eV, for XPS (where 0.2 eV represents the lifetime broadening of the Mg $K\alpha$ line). The instrumental resolution (Sec. II) was taken into account by broadening with a Gaussian function.

Figure 3 shows a comparison between the calculated and experimental spectra for XPS, He II UPS, and He I UPS. The calculation reproduces the energy positions and the photon energy dependence of the spectral features from -3 to -10 eV. Near the Fermi level (E_F), i.e., from 0 to -1 eV, however, there remains a discrepancy in the intensities of the spectra. The calculated intensity is too strong compared to the experimental spectra. Also, the weak struc-

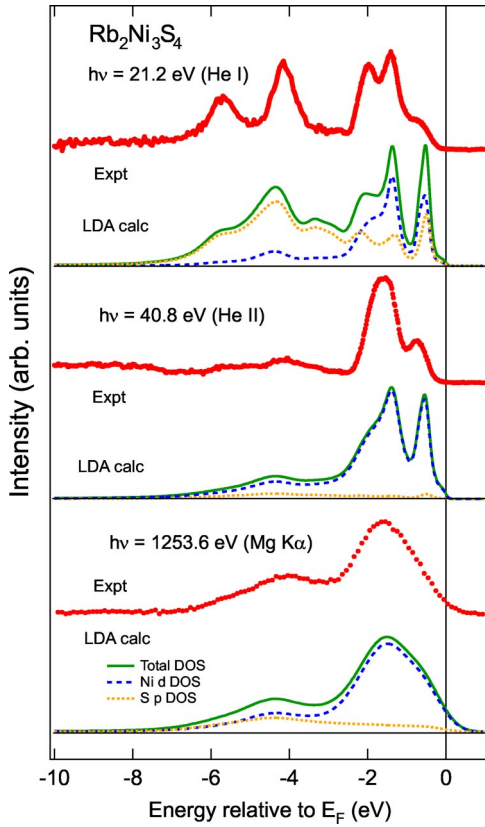


FIG. 3. (Color online) Comparison of the valence-band photoemission spectra with the LDA band-structure calculation. Contributions from the Ni d and S p partial DOS's are also shown.

ture F (at ~ -8 eV) is not reproduced by the calculation. These discrepancies may be attributed to electron correlation effects arising from the Coulomb repulsion between Ni $3d$ electrons, which cannot be properly taken into account in LDA calculations.

In order to treat correlation effects explicitly, we also simulated the valence-band spectra using a configuration-interaction (CI) calculation on a square planar $[\text{NiS}_4]^{6-}$ cluster model, which simulates the local environment of the Ni atom in $\text{Rb}_2\text{Ni}_3\text{S}_4$ (see Fig. 1). We assumed that the ground state of the cluster is the low-spin ($S=0$) state.¹² The ground-state wave functions of the cluster are given by linear combinations of the d^n , $d^{n+1}\underline{L}$, $d^{n+2}\underline{L}^2$, . . . configurations, where \underline{L} stands for a hole in the ligand S $3p$ orbitals. The model contains the following parameters: the on-site $3d$ - $3d$ Coulomb interaction energy U , the p -to- d charge-transfer energy defined by $\Delta = E(d^{n+1}) - E(d^n\underline{L})$, where $E(d^n\underline{L}^m)$ is the center of gravity of the $d^n\underline{L}^m$ multiplet, and the Slater-Koster parameter $(pd\sigma)$. The multiplet splitting of the Ni ion is expressed using Racah parameters B and C , which are fixed at the values of the free Ni^{2+} ion.¹⁶ One-electron transfer integrals between the Ni $3d$ and S ligand $3p$ orbitals are expressed in terms of the Slater-Koster parameters $(pd\sigma)$ and $(pd\pi)$. We have utilized the relationship $(pd\sigma)/(pd\pi) \approx -2$.¹⁷

The top panel of Fig. 4 shows the best fit result for the He II spectrum obtained with $\Delta = 0.6$ eV, $U = 3.5$ eV, and

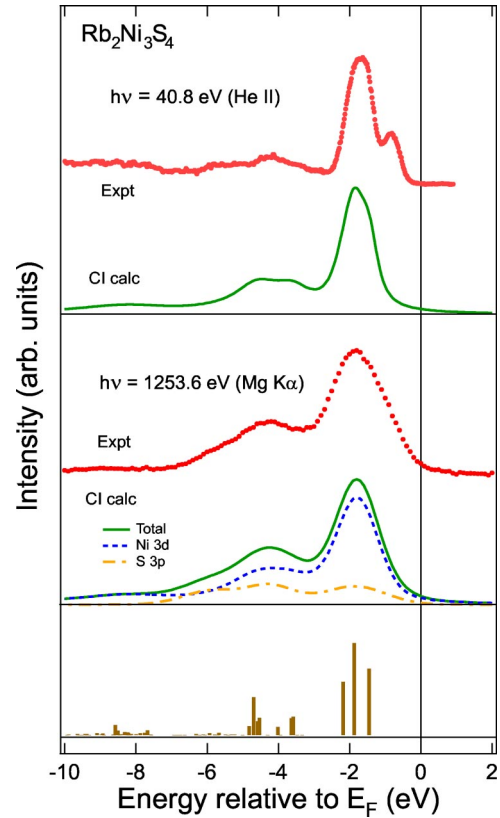


FIG. 4. (Color online) CI cluster-model analysis of the valence-band photoemission spectra. Top: He II UPS spectrum (dots) compared with the Ni $3d$ contribution. Middle: XPS spectrum compared with the Ni $3d$ plus S $3p$ contributions. Bottom: Line spectrum indicating the Ni $3d$ contribution without broadening. The parameter values are $\Delta = 0.6$ eV, $U = 3.5$ eV, and $(pd\sigma) = -1.35$ eV.

$(pd\sigma) = -1.35$ eV. For this photon energy, the S $3p$ cross section is negligibly small compared to that of Ni $3d$ due to the Cooper-minimum effect. We have convoluted the calculated line spectrum (the bottom panel of Fig. 4) using a Gaussian of FWHM ≈ 0.3 eV and a Lorentzian as described above. The calculated spectrum also reproduces the weak structure F at ~ -8 eV, which we attribute to a correlation satellite. However, the peak at -0.8 eV is not sufficiently split off from the other peaks in the calculated spectrum. The origin of this discrepancy is not known at present. We also calculated the valence-band XPS spectrum using the same parameter set as shown in the middle panel of Fig. 4. In order to compare the experimental data with the calculation, we changed the broadening parameters in order to take into account the lower energy resolution (Gaussian FWHM ≈ 1.0 eV). The contribution of the S $3p$ band to the XPS spectrum was estimated as follows: after having subtracted the background from the He I and He II spectra and normalized them by taking into account the relative cross sections of the atomic orbitals,¹⁴ we obtained the difference spectrum between the He I and He II spectra so that the Ni $3d$ contribution was cancelled out.

Figure 5 shows the XPS spectrum of the Ni $2p$ core level. The spectrum shows the spin-orbit doublet of $j = 3/2$ and $1/2$,

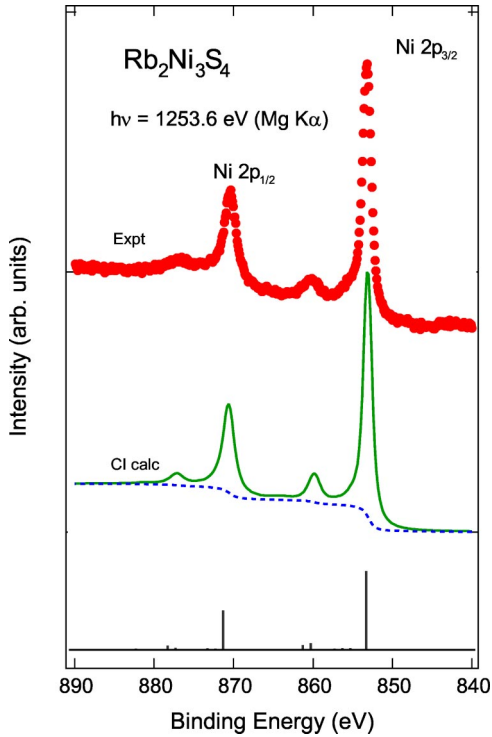


FIG. 5. (Color online) XPS spectrum of the Ni $2p$ core level and its CI cluster-model analysis. The integral background is given by the dashed curve. The bottom panel shows the calculated line spectrum without broadening. The parameter values are $\Delta=0.6$ eV, $U=3.5$ eV, $(pd\sigma)=-1.35$ eV, and $Q=4.1$ eV.

each component of which shows a charge-transfer satellite on the higher-binding-energy side separated by ~ 6 eV, corresponding to the satellite at ~ -8 eV in the valence-band spectra. We calculated the spectrum using the CI cluster model with the same parameter values for Δ , U , and $(pd\sigma)$ as those used for the valence band. In addition, the attractive Coulomb interaction between the Ni $2p$ core hole and the Ni $3d$ electron, $Q=4$ eV, was considered. The ratio $U/Q=0.87$ is close to ≈ 0.83 employed in Ref. 18.

In order to see both the occupied and unoccupied parts of the electronic structure, we made a combined plot of the XPS and BIS spectra in Fig. 6. In the figure, we also show theoretical spectra deduced from the LDA band-structure calculation and the CI cluster-model calculation. From comparison between theory and experiment, the dominant peak at ~ 2.0 eV above E_F in the BIS spectrum is found to be mainly of Ni $3d$ character with some hybridized S $3p$ character. However, the peak position in both calculations is shifted toward lower energies by ~ 1 eV compared to the experiment. Usually, a LDA calculation yields too low energy positions for unoccupied states and inaccurate energy positions for localized states, because density-functional theory (DFT), on which band theory is based, is strictly valid for the ground state, and further LDA uses the exchange-correlation energy of the homogeneous electron gas. That the present LDA and CI calculations predict the BIS peak position equally too low can be understood if the gap between the occupied and unoccupied states is determined by hybridization between Ni $3d$ and S $3p$ rather than the Ni $d-d$ Coulomb interaction. In

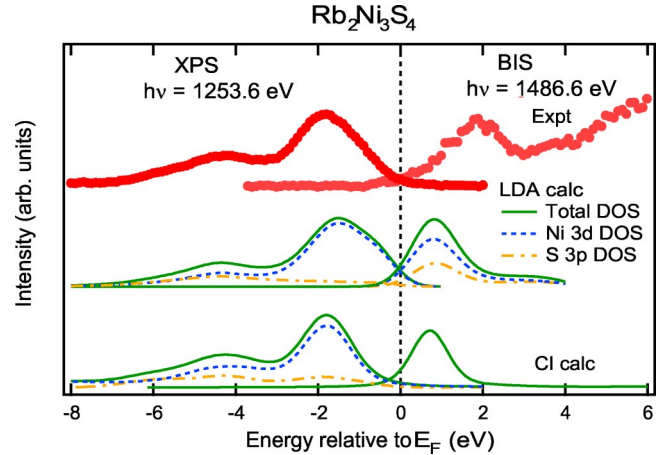


FIG. 6. (Color online) Combined XPS and BIS spectra in the valence-band region compared with the LDA band-structure and the CI cluster-model calculations.

fact, the indirect band gap of 0.66 eV given by the LDA band-structure calculation is in rather good agreement with the experimental value of 0.8 eV deduced from a transport study.¹² The photoemission and BIS spectra are consistent with a band gap of 0.5–1 eV, although it is difficult to accurately estimate the band gap because of the low energy resolution of BIS.

The parameter values deduced here, $\Delta=0.6$ eV, $U=3.5$ eV, and $(pd\sigma)=-1.35$ eV, are physically reasonable: the $(pd\sigma)$ value is close to those obtained for other divalent Ni-S compounds, such as -1.4 eV for hexagonal NiS (Ref. 20), -1.5 eV for pyrite-type NiS₂ (Ref. 19), and -1.5 eV for layered BaNiS₂ (Ref. 21). The U value is also similar to $U=4.0$ eV for NiS,²⁰ $U=3.3$ eV for NiS₂,¹⁹ and $U=3.0$ eV for BaNiS₂.²¹ On the other hand, the charge-transfer energy Δ varies significantly between these compounds: $\Delta=0.6$ eV for Rb₂Ni₃S₄ is remarkably smaller than those for NiS (2.5 eV) (Ref. 20) and NiS₂ (1.8 eV),¹⁹ but is similar to that for BaNiS₂ (1.0 eV).²¹ It has been reported for Ni oxides that Δ is influenced by the crystal structure; in particular, it is reduced with reduced dimensionality of the crystal.²²

Using the CI cluster model, one can analyze the ground-state wave function in terms of various electron configurations. The d^8 , $d^9\bar{L}$, and $d^{10}\bar{L}^2$ configurations are found to constitute 25%, 60%, and 15% of the low-spin ($S=0$) ground state of the $[\text{NiS}_4]^{6-}$ cluster. The d occupancy is thus found to be $n_d=8.90$, which is much larger than the ionic value 8 of the Ni²⁺ ion, indicating the highly covalent character of the Ni $3d$ -S $3p$ bonds. In order to see the origin of the spectral features, we decomposed the wave functions of the final states into various electron configurations (d^7 , $d^8\bar{L}$, $d^9\bar{L}^2$). In the region $-(1-3)$ eV, the main peak has dominant $d^8\bar{L}$ character and some $d^9\bar{L}^2$ contribution with a small contribution of d^7 . In the region $-(3-7)$ eV, the final states have dominant $d^9\bar{L}^2$ character and some $d^8\bar{L}$. In the region $-(7-10)$ eV, the weak satellite structure has some $d^9\bar{L}^2$ and $d^8\bar{L}$ character with a significant contribution from d^7 . For the parameter set used, the low-spin ($S=0$) state is found to be 0.59 eV below the high-spin ($S=1$) state. With decreas-

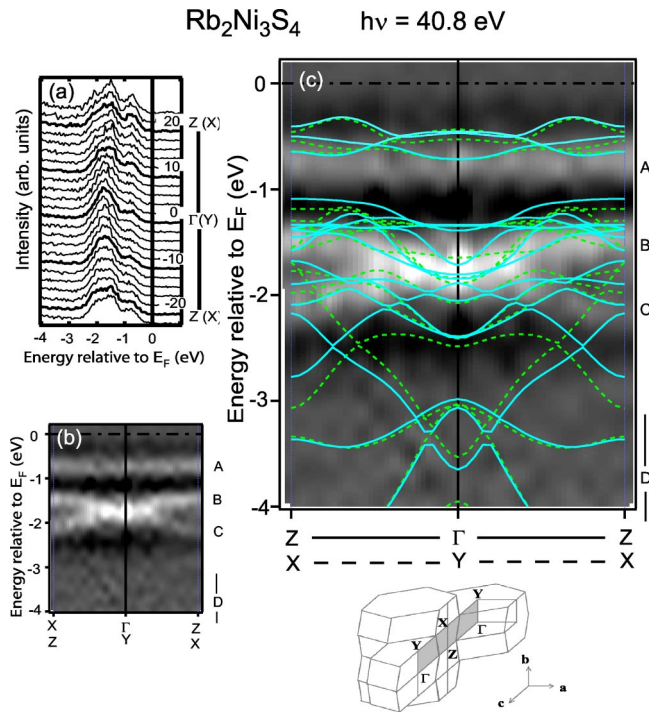


FIG. 7. (Color online) ARPES spectra of $\text{Rb}_2\text{Ni}_3\text{S}_4$. (a) Energy distribution curves (EDC's). The number on the right-hand side of each spectrum denotes the photoelectron take-off angle relative to the surface normal. (b) Gray-scale plot of the second derivatives of the EDC's in the energy-momentum space along the $\Gamma(Y)$ - $Z(X)$ direction. (c) Comparison with band-structure calculation. Bottom panel: Brillouin zone for $\text{Rb}_2\text{Ni}_3\text{S}_4$.

ing Δ or with increasing ($pd\sigma$), the low-spin state was found to be further stabilized relative to the high-spin state.

Finally, we present ARPES spectra to see to what extent the observed band dispersions in $\text{Rb}_2\text{Ni}_3\text{S}_4$ can be reproduced by the LDA band-structure calculation. Figure 7 shows the ARPES spectra measured with $h\nu=40.8$ eV for electron momentum \mathbf{k} in the plane along the $\Gamma(Y)$ - $Z(X)$ axis of the Brillouin zone. As mentioned above, the bands from -0.5 eV to -2.5 eV (A to C) are derived mainly from Ni $3d$ states. The remaining bands below -3 eV (D) are derived mainly from S $3p$ states. In Fig. 7(b), the second derivatives of the energy distribution curves (EDC's) [Fig. 7(a)] are displayed in a gray-scale plot. Here, the lighter color indicates a negative second derivative, namely, peaks

in the EDC's. The band at -0.8 eV (A) is seen to be almost dispersionless, while the bands from -1.5 eV to -2.2 eV (B and C) show appreciable \mathbf{k} dispersions. The bands below -2.5 eV show very weak intensities because of the low photoionization cross sections of the S $3p$ states, although they show strong dispersion. In Fig. 7(c), the calculated band dispersions are superimposed on the gray-scale plot. The solid curves indicate bands along the Z - Γ - Z line and the dashed curves those along the X - Y - X line. In the entire energy range, the experimental and calculated band dispersions show rather good correspondence. However, for band A, the calculation shows finite dispersion whereas the experiment does not show appreciable dispersion. As this band is almost purely Ni $3d$ -like, we consider that electron correlation effects for Ni $3d$ electrons are responsible for the discrepancy between theory and experiment.

IV. CONCLUSION

We have studied the electronic structure of $\text{Rb}_2\text{Ni}_3\text{S}_4$ by photoemission spectroscopy and compared the results with a LDA band-structure calculation and a CI cluster-model calculation. The band-structure calculation reproduced the gross features of the experimental spectra as well as the \mathbf{k} dispersions of S $3p$ -derived and Ni $3d$ -S $3p$ hybridized bands, but could not reproduce the weak satellite feature around -8 eV. The band-structure calculation also overestimated the intensity of the Ni $3d$ -derived band just below E_F , and failed to predict the dispersion of the same band in ARPES spectra. The CI cluster-model calculation well described the global behavior of the valence band and the Ni $2p$ core-level spectrum including the satellite structures, while it failed to predict the position of the peak at -0.8 eV. Therefore, we conclude that the actual electronic structure of $\text{Rb}_2\text{Ni}_3\text{S}_4$ is intermediate between the weak correlation limit described by the LDA band-structure calculation and the strong correlation limit as described by the CI cluster-model calculation, and is characterized by the strong hybridization between the Ni $3d$ and S $3p$ states.

ACKNOWLEDGMENTS

An enlightening discussion with D. D. Sarma is gratefully acknowledged. This work was supported by a Grant-in-Aid for Scientific Research in the Priority Area "Novel Quantum Phenomena in Transition-Metal Oxides" from the Ministry of Education, Culture, Sports, Science and Technology.

*Present address: Synchrotron Radiation Research Center, Japan Atomic Energy Research Institute, SPring-8, Mikazuki, Hyogo 679-5148, Japan.

¹M. Imada, A. Fujimori, and Y. Tokura, *Rev. Mod. Phys.* **70**, 1039 (1998).

²M. Matoba, S. Anzai, and A. Fujimori, *J. Phys. Soc. Jpn.* **60**, 4230 (1991).

³S. Miyasaka, H. Takagi, Y. Sekine, H. Takahashi, N. Mōri and R. J. Cava, *J. Phys. Soc. Jpn.* **69**, 3166 (2000).

⁴L. S. Martinson, J. W. Schweitzer, and N. C. Baenziger, *Phys. Rev. Lett.* **71**, 125 (1993).

⁵W. Bronger, R. Rennau, and D. Schmitz, *Z. Anorg. Allg. Chem.* **597**, 27 (1991).

⁶K. Mizushima, P. C. Jones, P. J. Wiseman, and J. B. Goodenough, *Mater. Res. Bull.* **15**, 783 (1980).

⁷C. Delmas and I. Saadoune, *Solid State Ionics* **53-57**, 370 (1992).

⁸W. Bronger, J. Eyck, W. Rudorff, and A. Stossel, *Z. Anorg. Allg. Chem.* **375**, 1 (1970).

⁹S. H. Elder, S. Jobic, R. Brec, M. Gelabert, and F. J. DiSalvo, *J. Alloys Compd.* **235**, 135 (1996).

¹⁰T. Kato, K. Hondou, and K. Iio, *J. Magn. Magn. Mater.* **177-181**, 591 (1998).

- ¹¹T. Fukamachi, Y. Kobayashi, A. Nakamura, H. Harashina, and M. Sato, *J. Phys. Soc. Jpn.* **68**, 3668 (1999).
- ¹²K. Hondou, Y. Fujiwara, T. Kato, K. Iio, A. Saiki, M. Usuda, and N. Hamada, *J. Alloys Compd.* **333**, 274 (2002).
- ¹³K. Takada, H. Sakurai, E. Takayama-Muromachi, F. Izumi, R. A. Dilanian, and T. Sasaki, *Nature (London)* **422**, 53 (2003).
- ¹⁴J. J. Yeh and I. Lindau, *At. Data Nucl. Data Tables* **32**, 1 (1985).
- ¹⁵A. Fujimori, M. Sekita, and H. Wada, *Phys. Rev. B* **33**, 6652 (1986).
- ¹⁶Y. Tanabe and S. Sugano, *J. Phys. Soc. Jpn.* **9**, 766 (1954).
- ¹⁷W. A. Harrison, *Electronic Structure and Physical Properties of Solids* (Freeman, San Francisco, 1980).
- ¹⁸A. E. Bocquet, T. Mizokawa, T. Saitoh, H. Namatame, and A. Fujimori, *Phys. Rev. B* **46**, 3771 (1992).
- ¹⁹A. Fujimori, K. Mamiya, T. Mizokawa, T. Miyadai, T. Sekiguchi, H. Takahashi, N. Mori, and S. Suga, *Phys. Rev. B* **54**, 16329 (1996).
- ²⁰S. R. Krishnakumar, N. Shanthi, P. Mahadevan, and D. D. Sarma, *Phys. Rev. B* **61**, 16 370 (2000).
- ²¹S. R. Krishnakumar, T. Saha-Dasgupta, N. Shanthi, P. Mahadevan, and D. D. Sarma, *Phys. Rev. B* **63**, 045111 (2001).
- ²²K. Maiti, P. Mahadevan, and D. D. Sarma, *Phys. Rev. B* **59**, 12457 (1999).